Yoshimoto and Yamanaka *Earth, Planets and Space* 2014, **66**:152
http://www.earth-planets-space.com/66/1/152

Earth, Planets and Space
a SpringerOpen Journal

LETTER Open Access

Teleseismic inversion of the 2004 Sumatra-Andaman earthquake rupture process using complete Green's functions

Masahiro Yoshimoto* and Yoshiko Yamanaka

Abstract

Spatial and temporal variations in coseismic slip distribution are often obtained by rupture process analyses using teleseismic body waves. Many analyses using teleseismic body waves were based on the ray theory because of the very efficiently computable direct P-, S-, and major reflected waves near the source. The 2004 Sumatra-Andaman earthquake was one of the largest earthquakes recorded in history, and the data that are required for the entire rupture process analysis include later phases such as PP waves and a very long period phase called a W phase. However, calculating these later phases using the conventional ray theoretical method is difficult. Here we investigate the rupture process of the 2004 Sumatra-Andaman earthquake using complete Green's functions, including all later phases such as PP waves and W phase. We use the direct solution method, which computes complete synthetic seismograms up to 2 Hz for transversely isotropic spherically symmetric media, to calculate the Green's functions. The obtained synthetic seismograms generated fit the observed seismograms quite well from a short period to a long period. The estimated slip distribution consists of four large slip areas: the largest slip occurred in the shallow part off the Sumatra west coast with a maximum slip of approximately 29 m, the second and third largest slips occurred in the shallow and deep parts of the Nicobar region with maximum slips of approximately 8 m and 7 m, respectively, and the fourth slip occurred in the middle Andaman region with a maximum slip of approximately 6 m. The estimated average rupture velocity is 2.8 km/s, but the rupture may have slowed between the Sumatra and the shallow Nicobar slip areas, and between the Nicobar and the middle Andaman slip areas. The delayed initiation of the shallow slips in the Nicobar region may possibly have been triggered by the deeper slip in the Nicobar region. There were no distinct depth-varying properties for the shallow and deep slips in the Nicobar region, as were reported for the 2011 Tohoku-Oki and 2010 Chile earthquake.

Keywords: Finite fault inversion; Teleseismic body waves; 2004 Sumatra-Andaman earthquake; Direct solution method

Correspondence/Findings

Introduction

The 26 December 2004 Sumatra-Andaman earthquake was one of the largest earthquakes ever to be instrumentally recorded; it caused the Indian Ocean tsunami, which killed over 250,000 people. Many high-quality geophysical data sets have led to a large number of proposed rupture models. This earthquake had a very long fault length of 1,200 to 1,300 km with a moment magnitude of 9.1 to 9.3 (Ammon et al. 2005; Stein and Okal 2005; Tsai et al. 2005). The source duration and rupture velocity were estimated to be approximately 500 s and 2 to 3 km/s, respectively, by high-frequency seismic and hydroacoustic data (Guilbert et al. 2005; Ishii et al. 2005; Ni et al. 2005; Tolstoy and Bohnenstiehl 2005).

Spatial and temporal variations in coseismic slip distribution are often obtained by rupture process analyses using teleseismic body waves. Many analyses of teleseismic body waves with short periods (in seconds) were based on the ray theory (e.g., Kikuchi and Kanamori 2003) because of very efficiently computable direct P, S, and major reflected waves near the source. Conventional teleseismic body wave inversion using the global broadband seismic network can be immediately analyzed after the occurrence of large earthquakes. However, some

* Correspondence: yoshimoto@seis.nagoya-u.ac.jp
Graduate School of Environmental Studies, Nagoya University, Furo-cho, Chikusa-ku, Nagoya 464-8601, Japan

problems arise when these methods analyze that the total duration of a rupture process is longer than the time window between the later phase PP waves and the P waves, such as the 2004 Sumatra-Andaman earthquake (Ji 2005; Yagi 2005; Yamanaka 2005). These methods cannot accurately calculate later phases such as PP waves because such waves are complicated by the upper mantle structure. Furthermore, these conventional methods cannot explain the long-period (up to 1,000 s) W phase, which has been observed in the displacement records of huge earthquakes and can be explained as the superposition of the fundamental mode and several overtones of spheroidal modes or Rayleigh waves (Kanamori 1993; Kanamori and Rivera 2008).

The model III of Ammon et al. (2005), hereafter called Ammon-III, was employed to conduct finite fault inversion of the earthquake using long-period body waves and surface waves (20 to 2,000 s) with the spectral element method for a three-dimensional earth model. Such long-period waveforms constrain the general features of the rupture process. On the other hand, abrupt changes in the rupture velocity or slip magnitude radiate high-frequency seismic waveforms (Das and Aki 1977; Madariaga 1977). To obtain detailed characteristics, such as variations in the slip velocity or rupture velocity, it is important to use higher-frequency seismograms. The purpose of this study is to analyze the full duration rupture process of the 2004 Sumatra-Andaman earthquake using complete (including all later phases such as PP waves and W phase) Green's functions including high frequency (i.e., seismic frequency bands that are the same as those for conventional teleseismic body wave inversion methods). The Green's functions were calculated up to 1 Hz using the direct solution method (DSM; Geller and Ohminato 1994; Kawai et al. 2006), which computes complete synthetic seismograms for transversely isotropic, spherically symmetric media.

Data and methods

In this study, the Green's functions were calculated by the DSM for transversely isotropic, spherically symmetric media (Kawai et al. 2006). We used the DSM software published on the Internet (Takeuchi 2010). The DSM computes synthetic seismograms by directly solving the Galerkin weak form of the equation of motion. Note that this program does not use geometrical optics or Earth-flattening approximations but efficiently computes highly accurate synthetic seismograms up to 2 Hz in a spherically symmetric, transversely isotropic Earth model. Detailed derivations of the DSM and extension to transversely isotropic spherically symmetric media up to 2 Hz were provided by Geller and Ohminato (1994) and Kawai et al. (2006), respectively. In this study, we calculated the Green's functions in the period range from 1/4,096 to 1 Hz using the IASP91 earth model (Kennett and Engdahl 1991) and applied the waveform inversion scheme of Kikuchi et al. (2003). We consider that the IASP91 earth model is appropriated for the Sumatra region (Additional file 1: Figure S1). We imposed two constraints: non-negative rake direction (Lawson and Hanson 1974) and spatial smoothness of the slip distributions. The smoothing constraint value is determined by inspecting whether the synthetic waveforms restore distinct phases of the observed waveforms and whether the slip distribution is not complex.

We used 52 vertical components of teleseismic body wave records collected by the Data Management Center of the Incorporated Research Institutions for Seismology (IRIS-DMC) with an epicentral distance between 30° and 100° (Figure 1). We eliminated the instrumental response of these records, applied band-pass filtering between 1 and 600 s, interpolated at a sampling interval of 2 Hz, and converted ground displacement waveforms. Both deconvolution and band-pass filtering were implemented in the time domain described by Kanamori and Rivera (2008). Working in the time domain is useful for reducing instrumental drift and avoiding the effects of wrap-around. We used the observation records before S waves because the S waves were too large in amplitude compared with the phases before the S waves. If we use the observation data including the S waves, the variance between observations and synthetics will be determined almost exclusively by the fitting of the S waves (i.e., the fitting of the P wave and PP waves is of minimal importance for the variance).

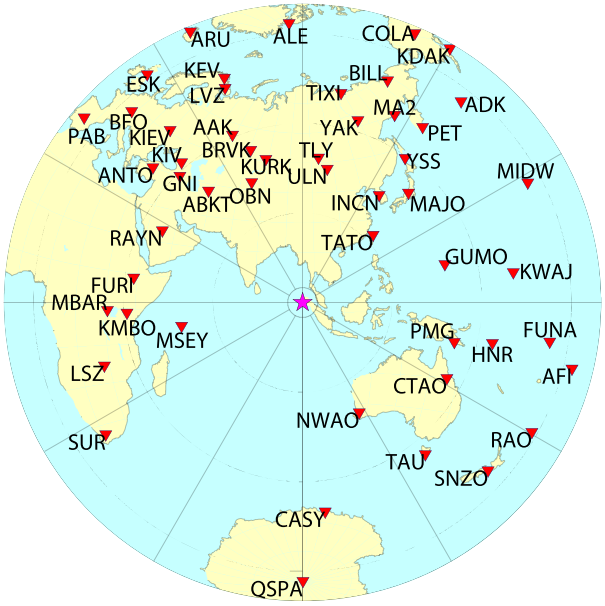

Figure 1 Broadband seismic stations used in the source inversion.

Teleseismic body wave inversion is a sensitive method for determining the depth of a slip area using the depth phases (i.e., the -pP and -sP phases). Ammon-III assumed three planar fault segments to express the very long and wide rupture area of the 2004 Sumatra earthquake; however, the subducting slab geometry obtained by seismicity is actually curved (Engdahl et al. 2007; Sibuet et al. 2007). The gap in depth between the assumed fault model and the true slab geometry causes a negative effect in the inversion results. It is important for teleseismic body wave inversion to use accurate fault geometry, particularly dip directions. Here we used the fault geometry model of Hoechner et al. (2008), which was constructed by an accurate discretization of subducting slab geometry. This fault geometry model consists of 12 × 36 = 432 subfaults with depths ranging from 5 to 53 km, based on regionalized upper mantle (RUM) slab geometry (Gudmundsson and Sambridge 1998). The average subfault length and width are 40 and 16 km, respectively. The detailed subfault parameters are cited in supplementary data set S3 of Hoechner et al. (2008). A single-point source is used as the subfault Green's function (i.e., rupture propagation inside each subfault is not included). The slip rate function of each grid point was expanded into 20 triangle functions with duration of 6 s at an interval of 3 s. We assumed a maximum rupture front velocity of 3.0 km/s, which was selected by a grid search between 1.0 and 4.0 km/s.

Results

The inversion results are shown in Figure 2. (Additional file 2: Figure S2 also shows the inversion results for an assumed maximum rupture front velocity of 2.0 and 4.0 km/s.) Figure 2a shows the obtained source time function. The total rupture duration is approximately 500 s, and the total seismic moment is 5.5×10^{23} Nm (Mw9.1). Figure 2b shows the slip distribution for an assumed maximum rupture front velocity of 3.0 km/s. The estimated slip distribution consists of four large slip areas: the largest slip area is located in the shallow part of the Sumatra region with a maximum slip of approximately 29 m (area A), the second and third areas of strong slip are located in the shallow and deep Nicobar region with maximum slips of approximately 8 and 7 m (areas B and C), respectively, and the fourth slip area is located in the middle depths of the Andaman region with a maximum slip of approximately 6 m (area D). The representative slip velocity function of each large slip area is also shown. Figure 3 shows a snapshot of the slip distribution at 20 s intervals. In the first 60 s, a small slip occurred near the hypocenter. After 60 s, the rupture of area A started to propagate to the northwest with an average rupture velocity of 3.0 km/s and lasted for 140 s (200 s after origin time). (Here, the average rupture velocity of each large slip area is defined to track the onset when the slip value reaches 2 m, which is approximately 30% of the maximum slip value for slip areas B, C, and D.) Then, the rupture of area C started to propagate to the north with an average rupture velocity of 3.0 km/s at 200 s. After 60 s from the start of rupture in area C (260 s after origin time), the rupture of area B also started to propagate to the north with an average rupture velocity of 4.0 km/s. The rupture of area B started 30 s after arrival of the assumed maximum rupture front at a velocity of 3.0 km/s. Although the ruptures of areas B and C both arrived in the Andaman region at 380 s, almost no slip occurred from 380 s to 460 s in the Andaman region. Finally, rupture occurred in area D from 460 s to 500 s. The rupture of area D started 40 s after arrival of the assumed maximum rupture front at a velocity of 3.0 km/s and propagated at an average rupture velocity of 3.0 km/s.

Discussion

Our source model using the DSM satisfactorily reproduces the features of the observed waveforms from short-period to long-period components (Figure 4). In particular, some station records with station azimuths between south and west (NWAO, CASY, QSPA, SUR, LSZ, MSEY, KMBO, MBAR, FURI, RAYN) clearly dominate the very long period components (W phase). These components cannot be calculated using conventional teleseismic body wave analyses (Yagi 2005; Yamanaka 2005; Ji 2005; see also Additional file 3: Figure S3) but are explained well with synthetics. For the distance between the rupture extent and the hypocenter (1,380 km) with the rupture duration (500 s), we obtained an average rupture velocity of approximately 2.8 km/s. These overall source parameters are consistent with other studies using seismic waves (Ammon et al. 2005; Ishii et al. 2005).

The large slip segments are in located in four separate areas. The transitions of each segment along the strike direction are roughly consistent with the changes the physical properties of the subducted slab from seismic tomography (Kennett and Cummins 2005). Although the average rupture velocities in areas A and C have the same value as the maximum rupture front velocity of 3.0 km/s, the rupture in areas B and D started 30 to 40 s after arrival of the assumed maximum rupture front at a velocity of 3.0 km/s and propagated with average rupture velocities of 4.0 and 3.0 km/s, respectively. The southern sides of areas B and D are not ruptured. These areas may form a barrier region (velocity-strengthening behavior), and the barriers may cause the rupture velocities to be slow. The slow rupture initiation in the shallow Nicobar region was further supported by a recent joint inversion of tide gauge, satellite altimetry, and GPS data by Lorito et al. (2010). The slow rupture velocity of the Andaman region has been indicated in many studies (e.g., de Groot-Hedlin 2005; Guilbert et al. 2005; Tolstoy and Bohnenstiehl 2005;

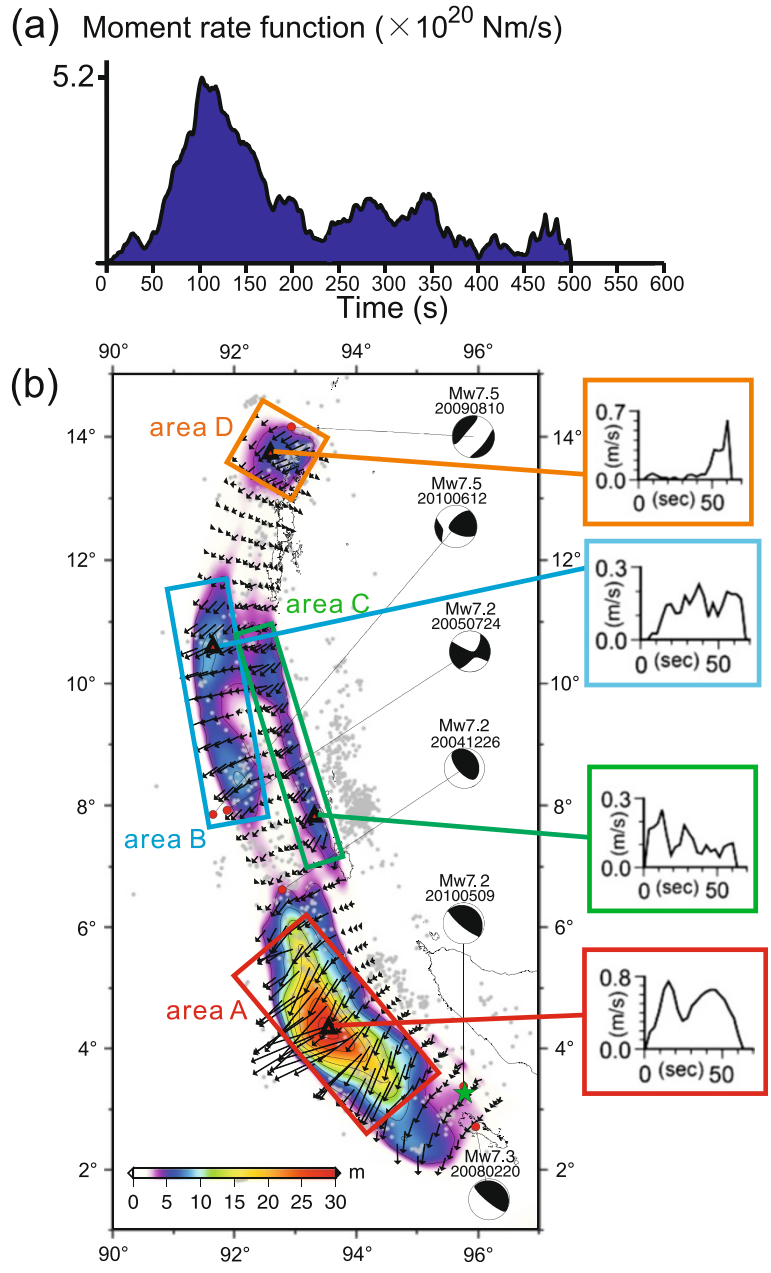

Figure 2 Inversion results. (a) Moment rate function. **(b)** Slip distribution on the fault. The green star represents the epicenter of the main shock, the red circles represent large aftershocks (Mw >7.0), and the gray circles represent aftershocks (Mw >5.0). The red, blue, green, and orange rectangles denote the large slip areas. The representative slip rate function of each slip area, at the location of the red triangles, is also shown. The beach balls show the focal mechanisms of the Global Centroid Moment Tensor catalog. The numbers above the focal mechanisms are the moment magnitude (top) and the date of occurrence (year, month, day; bottom). The slip contour interval in the slip distribution is 4 m.

Tsai et al. 2005). Another interpretation of the delay onset of slip with respect to the maximum rupture front in area B is that the slip in area B may have been triggered by the slip in area C.

Ammon et al. (2005) showed that three relatively energetic amplitude bursts (from 50 to 150, 280 to 340, and 450 to 500 s) can be identified in high-frequency seismograms. These energetic bursts correspond with the slip of our results in areas A, B and/or C, and D, respectively. Although the slip rate functions of areas A and D have large peak slip rate values and distinct peaks (the slip rate function of area A has two peaks), the variations of these functions for areas B and C are relatively moderate. Comparing the slip rate function in area B with that in area C, the slip rate in area B increases moderately and maintains the same value in the last time

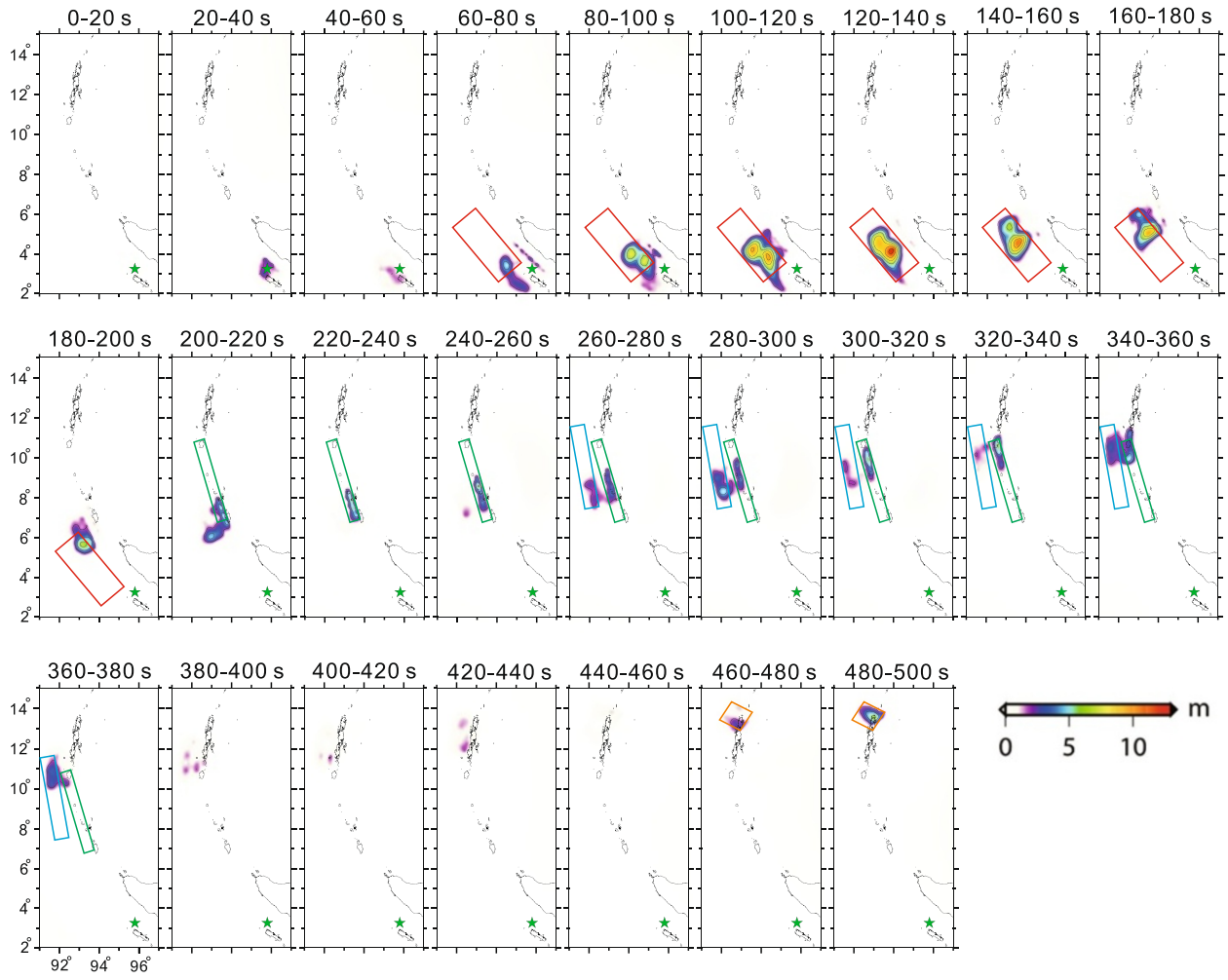

Figure 3 Snapshot of the rupture process at 20 s intervals. The contour interval is 2 m. The star represents the epicenter of the main shock. The colored rectangles denote large slip areas, as shown in Figure 2b.

window, but the slip rate in area C rises rapidly and decreases with time. These features may represent depth-varying rupture properties of the subduction zone (e.g., Lay et al. 2012); however, there are no distinct variables in these functions, which is in contrast to distinguish the properties reported in the 2011 Tohoku-Oki and 2010 Chile earthquakes (e.g., Asano and Iwata 2012; Koper et al. 2011, 2012; Wang and Mori 2011).

The obtained source time function is very similar to that of Ammon-III. A source time function is the most stable parameter despite some differences in fault parameters in finite fault inversion (e.g., Lay et al. 2010). The largest moment release occurred from 60 to 200 s in the Sumatra region (area A). This largest moment release in area A has been obtained in most rupture process analyses. The largest slip area of our study is located off the west coast of the Sumatra islands at a depth shallower than 30 km with a maximum slip of approximately 29 m. However, the largest slip area of Ammon-III is located in the deeper part of the Sumatra region with a maximum slip of approximately 12 m. Araki et al. (2006) deployed the ocean bottom seismographic network around this region in February and March 2005. The aftershock distribution was mainly concentrated deeper than 25 km, and their focal mechanisms were dominantly the dip-slip type. These aftershocks are considered to have occurred at the plate interface. In contrast, aftershocks at depths shallower than 25 km were dominantly by a dip-extension type mechanism. The large reverse fault mechanism aftershocks greater than Mw7.0 occurred on the edge of the largest slip area of our study (Figure 2b). This relation between large slip areas and aftershocks has already been indicated in previous studies (e.g., Mendoza and Hartzell 1988; Houston and Engdahl 1989), and this comparison indicates the robustness of the rupture process analysis. These results support the shallow largest slip of our result.

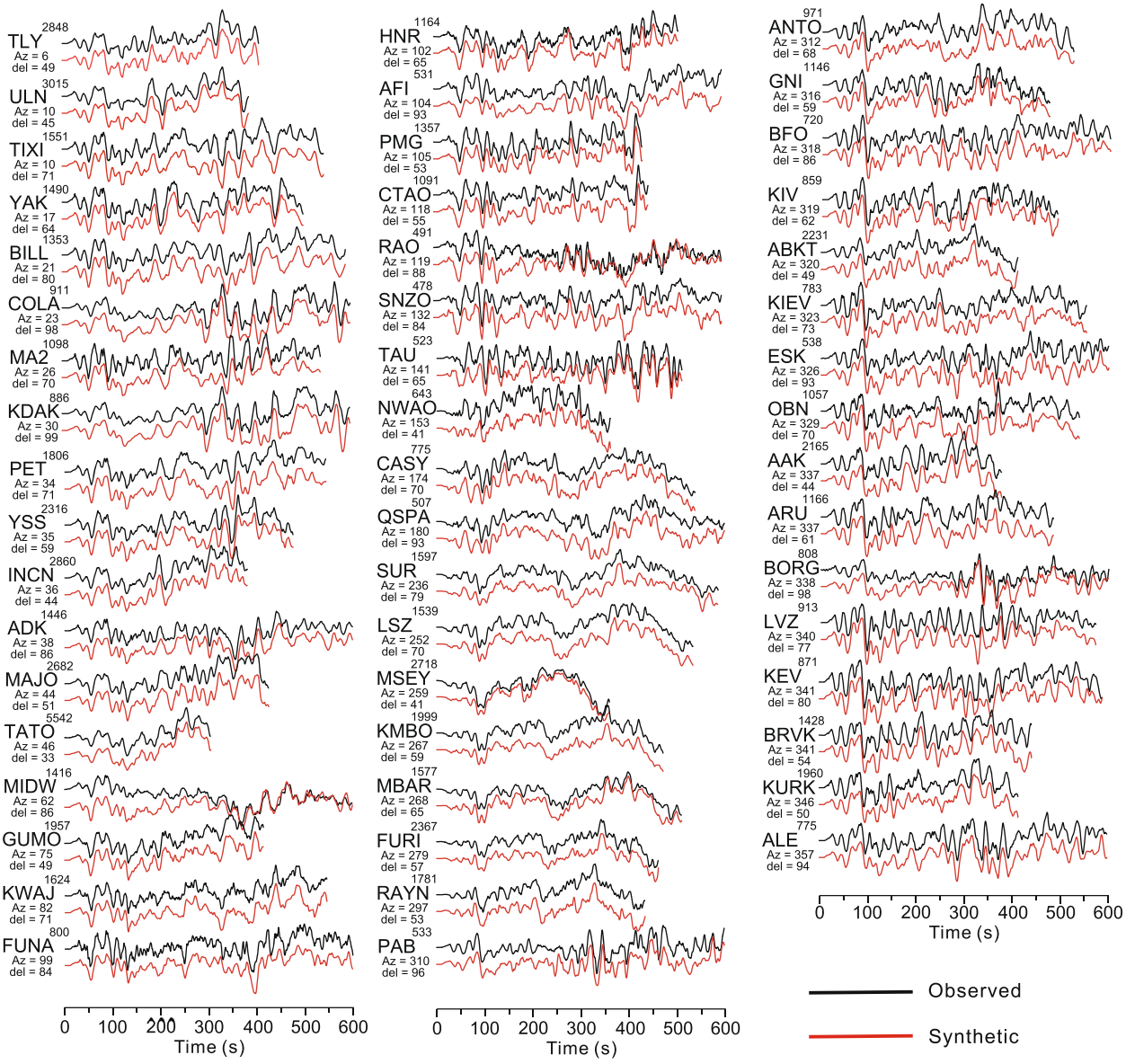

Figure 4 Comparison of the observed (black) and synthetic (red) seismograms. The number above the station code is the peak-to-peak amplitude of the observed waveform (micrometer), and the numbers below the station code indicate the source to station azimuth and the epicentral distance.

A significant discrepancy is present in the amount of maximum slip between our study and Ammon-III. This discrepancy was caused by the different rigidities between our study (30 GPa) and Ammon-III (68 GPa), because the largest slip area of our study is located in the shallow region. Seno and Hirata (2007) reported that the maximum slip of the tsunami models (approximately 30 m; e.g., Hirata et al. 2006; Tanioka et al. 2006; Fujii and Satake 2007) is generally larger than that of the seismological models (approximately 15 m; e.g., Ammon et al. 2005; Ji 2005; Yamanaka 2005). They suggested that additional crustal deformation, such as inelastic uplift of the trench sediments, might have occurred near the deformation front. However, the maximum slip value of our result is consistent with the tsunami models. This shows that no additional slip, such as inelastic deformation, is necessary.

Our results indicate that the rupture occurred in both shallow and deep parts of the Nicobar region (areas B and C); this result was further obtained by Lorito et al. (2010). Two large left lateral fault mechanism aftershocks (Mw7.2, Mw7.5) occurred in the Nicobar region. The depths of the aftershocks obtained by Global CMT were 12 and 33 km, respectively, and these aftershocks

were considered to be a reactivation of the fracture zone of the subducted oceanic plate triggered by the main shock. Unless the rupture occurred in the shallow near-trench region, a positive Coulomb stress change for the two aftershocks was not produced (Delescluse et al. 2012 On the other hand, the subsidences of approximately 3 m in the Nicobar Islands and Great Nicobar were not explained only by the shallow slip; to cause these subsidences, the deep part slip is necessary. These facts support both the shallow and deep part slips in the Nicobar region obtained by our result; however, these subsidences may be caused by not only coseismic slip but also postseismic slip in the deep part.

Next, the rupture propagated at 11° N near Little Andaman, and almost no slip occurred from 11° N to 13° N; however, a rupture occurred around 13° N to 14° N in the northern end (area D) 40 s after the arrival of the rupture front. The large normal fault mechanism aftershock (Mw7.5) in the Andaman region was considered to be an extension event caused by a slab pull force following the main shock (Andrade and Rajendran 2011).

Conclusions

We estimated the rupture process of the 2004 Sumatra-Andaman earthquake using teleseismic body waves. This was a giant earthquake with very long rupture duration of approximately 500 s; therefore, conventional teleseismic body wave analyses, which cannot calculate later phases such as PP waves and W phase, could not reveal the entire rupture process. Our source model satisfactorily reproduces the features of the observed waveforms, including later phases from short-period to long-period components. The largest slip area was determined to have been in the shallow Sumatra region with a maximum slip of approximately 29 m. The shallow largest slip is consistent with the large slip obtained by tsunami inversions and supported by the aftershock locations. Other slip areas were determined in the shallow and deep Nicobar region and Andaman region. Although the rupture started in the deep Nicobar region immediately after arrival of the assumed maximum rupture front velocity of 3.0 km/s, the beginning of rupturing in the shallow Nicobar region was delayed by 30 s and that in the Andaman regions was delayed by 40 s after this arrival. The southern areas of these delayed rupture initiations are not ruptured. These areas may a barrier region, and the rupture velocities are slow because of these barriers. Another interpretation of the delay onset of slip with respect to the maximum rupture front in the shallow Nicobar region is that the slip in shallow Nicobar region may have been triggered by the slip in the deeper Nicobar region. There were no distinct depth-varying properties of the shallow and deep slips in the Nicobar region.

Additional files

Additional file 1: Figure S1. Comparison of the synthetics with the observation of two moderate size earthquakes in the Sumatra region. **(a)** Location of the two moderate size earthquakes. The red and blue stars represent the epicenter of 26 February 2005 Sumatra region earthquake (Mw6.6) and 22 December 2006 Andaman region earthquake (Mw5.9), respectively. Waveform inversion results of the 2005 Sumatra earthquake using the IASP91 and a modified PREM velocity models are also shown. The modified Preliminary Reference Earth Model (PREM), which originally had a 3 km deep ocean layer, was adopted by replacing the ocean layer with the crust layer. **(b)** Comparison of the synthetics with observation of two moderate size earthquakes. The black, red, and green lines represent the observed, the synthetic with the IASP91, and the synthetic with the modified PREM, respectively. The numbers above and below the station code indicate the peak-to-peak amplitude in micrometers of the observation record and azimuth, respectively.

Additional file 2: Figure S2. Comparison of the inversion results for an assumed maximum rupture front velocity of 2.0 and 4.0 km/s.

Additional file 3: Figure S3. (Upper) Inversion results using the Green's functions, which are calculated by conventional ray theoretical method (Kikuchi and Kanamori 2003). The triangle shape and the numbers of the slip rate functions and maximum rupture front velocity are assumed same as that in the text. (Lower) Comparison of the correlation coefficient (CC) of the synthetic and observed waveforms with the different period range. The star and circle indicate the results using the synthetics with this study and Kikuchi and Kanamori (2003), respectively. The numbers of the horizontal axis indicate the period range of applied band-pass filter (BP). The numbers of 1, 2, 3, and 4 of BP represent the period range from 1 to 600, from 50 to 200, from 100 to 600, and from 200 to 600 s, respectively.

Competing interests

The authors declare that they have no competing interests.

Authors' contributions

MY carried out the inversion analysis and wrote the manuscript. YY provided valuable help to interpret the results and reviewed the manuscript. Both authors read and approved the final manuscript.

Acknowledgements

For this study, we used the computer systems of the Earthquake Information Center of the Earthquake Research Institute, University of Tokyo. This study was supported by the Earthquake Research Institute cooperative research program. We thank Nozomu Takeuchi for helpful comments on using the DSM program. The authors would like to thank Enago (www.enago.jp) for the English language review. We appreciate Hiroshi Takenaka and two anonymous reviewers for their helpful comments and suggestions for improving this manuscript.

Received: 20 January 2014 Accepted: 29 October 2014
Published online: 18 November 2014

References

Ammon CJ, Ji C, Thio H-K, Robinson D, Ni S, Hjorleifsdottir V, Kanamori H, Lay T, Das S, Helmberger D, Ichinose G, Polet J, Wald D (2005) Rupture process of the 2004 Sumatra-Andaman earthquake. Science 308(5725):1133–1139, doi:10.1126/science.1112260

Andrade V, Rajendran K (2011) Intraplate response to the great 2004 Sumatra-Andaman earthquake: a study from the Andaman segment. Bull Seismol Soc Am 101(2):506–514, doi:10.1785/0120100155

Araki E, Shinohara M, Obana K, Yamada T, Kaneda Y, Kanazawa T, Suyehiro K (2006) Aftershock distribution of the 26 December 2004 Sumatra-Andaman earthquake from ocean bottom seismographic observation. Earth Planets Space 58(2):113–119

Asano K, Iwata T (2012) Source model for strong ground motion generation in the frequency range 0.1–10 Hz during the 2011 Tohoku earthquake. Earth Planets Space 64:1111–1123, doi:10.5047/eps.2012.05.003

Das S, Aki K (1977) Fault plane with barriers-versatile earthquake model. J Geophys Res 82(36):5658–5670, doi:10.1029/Jb082i036p05658

de Groot-Hedlin CD (2005) Estimation of the rupture length and velocity of the Great Sumatra earthquake of Dec 26, 2004 using hydroacoustic signals. Geophys Res Lett 32(11):L11303, doi:10.1029/2005GLO22695

Delescluse M, Chamot-Rooke N, Cattin R, Fleitout L, Trubienko O, Vigny C (2012) April 2012 intra-oceanic seismicity off Sumatra boosted by the Banda-Aceh megathrust. Nature 490(7419):240–244, doi:10.1038/Nature11520

Engdahl ER, Villasenor A, DeShon HR, Thurber CH (2007) Teleseismic relocation and assessment of seismicity (1918-2005) in the region of the 2004 M-w 9.0 Sumatra-Andaman and 2005 M-w 8.6 Nias Island great earthquakes. Bull Seismol Soc Am 97(1):S43–S61, doi:10.1785/0120050614

Fujii Y, Satake K (2007) Tsunami source of the 2004 Sumatra-Andaman earthquake inferred from tide gauge and satellite data. Bull Seismol Soc Am 97(1):S192–S207, doi:10.1785/0120050613

Geller RJ, Ohminato T (1994) Computation of synthetic seismograms and their partial derivatives for heterogeneous media with arbitrary natural boundary-conditions using the direct solution method. Geophys J Int 116(2):421–446, doi:10.1111/j.1365-246X.1994.tb01807.x

Gudmundsson O, Sambridge M (1998) A regionalized upper mantle (RUM) seismic model. J Geophys Res 103(B4):7121–7136, doi:10.1029/97jb02488

Guilbert J, Vergoz J, Schissele E, Roueff A, Cansi Y (2005) Use of hydroacoustic and seismic arrays to observe rupture propagation and source extent of the Mw =9.0 Sumatra earthquake. Geophys Res Lett 32(15):L15310, doi:10.1029/2005GL022966

Hirata K, Satake K, Tanioka Y, Kuragano T, Hasegawa Y, Hayashi Y, Hamada N (2006) The 2004 Indian Ocean tsunami: tsunami source model from satellite altimetry. Earth Planets Space 58(2):195–201

Hoechner A, Babeyko AY, Sobolev SV (2008) Enhanced GPS inversion technique applied to the 2004 Sumatra earthquake and tsunami. Geophys Res Lett 35(8):L08310, doi:10.1029/2007gl033133

Houston H, Engdahl ER (1989) A comparison of the spatio-temporal distribution of moment release for the 1986 Andreanof Islands earthquake with relocated seismicity. Geophys Res Lett 16(12):1421–1424, doi:10.1029/Gl016i012p01421

Ishii M, Shearer PM, Houston H, Vidale JE (2005) Extent, duration and speed of the 2004 Sumatra-Andaman earthquake imaged by the hi-net array. Nature 435(7044):933–936, doi:10.1038/Nature03675

Ji C (2005) Magnitude 9.1 off the west coast of northern Sumatra. Sunday, December 26, 2004 at 00:58:53 UTC. http://neic.usgs.gov/neis/eq_depot/2004/eq_041226/neic_slav_ff.html. Accessed 2 Dec 2013

Kanamori H (1993) W phase. Geophys Res Lett 20(16):1691–1694, doi:10.1029/93gl01883

Kanamori H, Rivera L (2008) Source inversion of W phase: speeding up seismic tsunami warning. Geophys J Int 175(1):222–238, doi:10.1111/j.1365-246X.2008.03887.x

Kawai K, Takeuchi N, Geller RJ (2006) Complete synthetic seismograms up to 2 Hz for transversely isotropic spherically symmetric media. Geophys J Int 164(2):411–424, doi:10.1111/j.1365-246X.2005.02829.x

Kennett BLN, Cummins PR (2005) The relationship of the seismic source and subduction zone structure for the 2004 December 26 - Sumatra-Andaman earthquake. Earth Planet Sci Lett 239(1–2):1–8, doi:10.1016/j.epsl.2005.08.015

Kennett BLN, Engdahl ER (1991) Traveltimes for global earthquake location and phase identification. Geophys J Int 105(2):429–465, doi:10.1111/j.1365-246X.1991.tb06724.x

Kikuchi M, Kanamori H (2003) Note on teleseismic body-wave inversion program. http://www.eri.u-tokyo.ac.jp/ETAL/KIKUCHI/

Kikuchi M, Nakamura M, Yoshikawa K (2003) Source rupture processes of the 1944 Tonankai earthquake and the 1945 Mikawa earthquake derived from low-gain seismograms. Earth Planets Space 55:159–172

Koper KD, Hutko AR, Lay T, Ammon CJ, Kanamori H (2011) Frequency-dependent rupture process of the 2011 *Mw*9.0 Tohoku earthquake: comparison of short-period *P* wave backprojection images and broadband seismic rupture models. Earth Planets Space 63:599–602, doi:10.5047/eps.2011.05.026

Koper KD, Hutko AR, Lay T, Sufri O (2012) Imaging short-period seismic radiation from the 27 February 2010 Chile (*Mw* 8.8) earthquake by backprojection of *P*, *PP*, and *PKIKP* waves. J Geophys Res 117:B02308, doi:10.1029/2011JB008576

Lawson CL, Hanson RJ (1974) Solving least squares problems. Prentice-Hall, Englewood Cliffs

Lay T, Ammon CJ, Kanamori H, Koper KD, Sufri O, Hukto AR (2010) Teleseismic inversion for rupture process of the 27 February 2010 Chile (Mw 8.8) earthquake. Geophys Res Lett 37:L13301, doi:10.1029/2010gl043379

Lay T, Kanamori H, Ammon CJ, Koper KD, Hukto AR, Ye L, Yue H, Rushing TM (2012) Depth-varying rupture properties of subduction zone megathrust faults. J Geophys Res 117:B04311, doi:10.1029/2011JB009133

Lorito S, Piatanesi A, Cannelli V, Romano F, Melini D (2010) Kinematics and source zone properties of the 2004 Sumatra-Andaman earthquake and tsunami: nonlinear joint inversion of tide gauge, satellite altimetry, and GPS data. J Geophys Res 115:B02304, doi:10.1029/2008jb005974

Madariaga R (1977) High-frequency radiation from crack (stress drop) models of earthquake faulting. Geophys J R Astron Soc 51(3):625–651, doi:10.1111/j.1365-246X.1977.tb04211.x

Mendoza C, Hartzell SH (1988) Aftershock patterns and main shock faulting. Bull Seismol Soc Am 78(4):1438–1449

Ni S, Kanamori H, Helmberger D (2005) Seismology: energy radiation from the Sumatra earthquake. Nature 434(7033):582, doi:10.1038/434582a

Seno T, Hirata K (2007) Did the 2004 Sumatra–Andaman earthquake involve a component of tsunami earthquakes? Bull Seismol Soc Am 97(1):S296–S306, doi:10.1785/0120050615

Sibuet JC, Rangin C, Le Pichon X, Singh S, Cattaneo A, Graindorge D, Klingelhoefer F, Lin JY, Malod J, Maury T, Schneider JL, Sultan N, Umber M, Yamaguchi H, Sumatra aftershocks Team (2007) 26th December 2004 great Sumatra–Andaman earthquake: co-seismic and post-seismic motions in northern Sumatra. Earth Planet Sci Lett 263(1–2):88–103, doi:10.1016/j.epsl.2007.09.005

Stein S, Okal EA (2005) Seismology: speed and size of the Sumatra earthquake. Nature 434(7033):581–582, doi:10.1038/434581a

Takeuchi N (2010) Direct solution method software. http://www.eri.u-tokyo.ac.jp/takeuchi/software/index.html

Tanioka Y, Yudhicara KT, Kathiroli S, Nishimura Y, Iwasaki SI, Satake K (2006) Rupture process of the 2004 great Sumatra-Andaman earthquake estimated from tsunami waveforms. Earth Planets Space 58(2):203–209

Tolstoy M, Bohnenstiehl DR (2005) Hydroacoustic constraints on the rupture duration, length, and speed of the great Sumatra-Andaman earthquake. Seismol Res Lett 76(4):419–425

Tsai VC, Nettles M, Esktrom G, Dziewonski AM (2005) Multiple CMT source analysis of the 2004 Sumatra earthquake. Geophys Res Lett 32(17):L17304, doi:10.1029/2005gl023813

Wang D, Mori J (2011) Frequency-dependent energy radiation and fault coupling for the 2010 Mw8.8 Maule, Chile, and 2011 Mw9.0 Tohoku, Japan, earthquakes. Geophys Res Lett 38:L22308, doi:10.1029/2011GL049652

Yagi Y (2005) Preliminary results of rupture process for 2004 Off Coast of Northern Sumatra Giant Earthquake (ver. 1). http://iisee.kenken.go.jp/staff/yagi/eq/Sumatra2004/Sumatra2004.html. Accessed 2 Dec 2013

Yamanaka Y (2005) Source process of the 2004 Sumatra earthquake. In: Abstracts of 2005 Japan earth and planetary science joint meeting, Makuhari Messe, Chiba, Japan, pp 22–26, May 2005

doi:10.1186/s40623-014-0152-4
Cite this article as: Yoshimoto and Yamanaka: **Teleseismic inversion of the 2004 Sumatra-Andaman earthquake rupture process using complete Green's functions.** *Earth, Planets and Space* 2014 **66**:152.